Exact Potential Driving the Electron Dynamics in Enhanced Ionization of H_2^+

Elham Khosravi,[1,2,*] Ali Abedi,[1,2,†] and Neepa T. Maitra[1,‡]
[1]Department of Physics and Astronomy, Hunter College and the Graduate Center of the City University of New York, 695 Park Avenue, New York, New York 10065, USA
[2]Nano-Bio Spectroscopy Group and European Theoretical Spectroscopy Facility (ETSF), Universidad del País Vasco CFM CSIC-UPV/EHU-MPC and DIPC, Av. Tolosa 72, 20018 San Sebastián, Spain
(Received 6 August 2015; published 29 December 2015)

It was recently shown that the exact factorization of the electron-nuclear wave function allows the construction of a Schrödinger equation for the electronic system, in which the potential contains exactly the effect of coupling to the nuclear degrees of freedom and any external fields. Here we study the exact potential acting on the electron in charge-resonance enhanced ionization in a model one-dimensional H_2^+ molecule. We show there can be significant differences between the exact potential and that used in the traditional quasistatic analyses, arising from nonadiabatic coupling to the nuclear system, and that these are crucial to include for accurate simulations of time-resolved ionization dynamics and predictions of the ionization yield.

DOI: 10.1103/PhysRevLett.115.263002 PACS numbers: 31.15.−p, 31.50.−x, 82.50.−m

Ionization is a fundamental process in strong-field physics, lying at the heart of many fascinating phenomena such as high harmonic generation, Coulomb explosion, and molecular orbital tomography. The ionization rate from a molecule can be several orders of magnitude higher than the rate from the constituent atoms at a critical range of internuclear separations. This phenomenon, termed charge-resonance enhanced ionization (CREI), was theoretically predicted [1–4] and verified experimentally [5–7]. The ionization rate enhancement has been explained by a quasistatic argument [2,4,8–11], treating the nuclei as instantaneously fixed point particles, with the electrons following the combined potential from the laser field and the electrostatic attraction to the nuclei. In any experiment, however, the nuclei are neither frozen, nor are they point particles; instead their motion can be *strongly* coupled to the electron dynamics and accounting for the coupled electron-ion quantum dynamics can be essential [12]. Further, the electron does not simply follow the field adiabatically, as revealed by the multiple subcycle ionization bursts [13,14]. Calculations treating the full quantum dynamics of the nuclei and electron in H_2^+ [4,8], and a few experiments, have verified that the essential CREI phenomenon remains robust, although ionic dynamics alter the details. For example, nuclear motion washes out the two-peak structure predicted in the frozen-nuclei analysis [2] into a single broad peak [5]. Further, CREI is subdued if, during the experiment, only little of the nuclear density reaches the critical internuclear separation [15]. Hence, to properly understand, model, and predict the experiment, a fully time-dependent (TD) picture of coupled electronic and ionic motion is needed.

Here, we utilize the exact factorization approach [16–29] to investigate the electron dynamics during CREI. In particular, we study the exact TD potential that drives the electron, introduced by the exact factorization in its reverse form [20], which fully accounts for coupling to both the field and the dynamical nuclei. This exact potential can be remarkably different from the quasistatic potential (ϵ^{qs}), or even from modifying ϵ^{qs} to account for the width and splitting of the nuclear wave packet. Therefore dynamical electron-nuclear correlation effects must be included in the calculation. Further, we identify a measure of ionization for fully dynamical studies indicating the regions of the nuclear wave packet associated with the ionizing electron.

Restricting the motion of the nuclei and the electron in the H_2^+ molecule to the polarization direction of the laser field, the problem can be modeled with a one-dimensional Hamiltonian featuring "soft-Coulomb" interactions [30] (atomic units are used throughout the article, unless otherwise noted):

$$\hat{H}(t) = -\frac{1}{2\mu_e}\frac{\partial^2}{\partial z^2} - \frac{1}{M}\frac{\partial^2}{\partial R^2} - \frac{1}{\sqrt{1+(z-R/2)^2}} - \frac{1}{\sqrt{1+(z+R/2)^2}} + \frac{1}{\sqrt{0.03+R^2}} + \hat{V}_l(z,t) \quad (1)$$

where R and z are the internuclear distance and the electronic coordinate as measured from the nuclear center-of-mass, respectively. M denotes the proton mass while $\mu_e = (2M)/(2M+1)$ is the electronic reduced mass. The laser field is $\hat{V}_l(z,t) = q_e z E(t)$ within the dipole approximation where $E(t)$ denotes the electric field amplitude and $q_e = (2M+2)/(2M+1)$. Such a model captures much of the physics of CREI; however, it cannot capture all the strong-field molecular phenomena, e.g. rotations that couple strongly via light-induced conical intersections [31].

First we study the dynamics of the system subject to a 50-cycle pulse of wavelength $\lambda = 800$ nm and intensity

$I = 2 \times 10^{14}$ W/cm^2, with a sine-squared pulse envelope. Choosing the ground state as the initial state, we first solve the TD Schrödinger equation (TDSE) numerically exactly. The upper panel of Fig. 1, shows the dissociation and ionization probability and the average internuclear distance versus number of optical cycles (t/T). (The laser period is $T = 2.67$ fs.) Ionization is rapidly onset as we approach the middle of the pulse, slowing down later while the field decreases. The nuclei dissociate primarily via Coulomb explosion following ionization. Most of the ionization occurs when the average internuclear separation $\langle R \rangle$ is between 4 and 5 a.u. The inset of the upper panel shows the ionization rate versus $\langle R \rangle(t)$ (fixed R) for fully dynamical (clamped-nuclei) calculation. For clamped-nuclei, the peak near 6.5 a.u. is usually identified with CREI while that near 5 a.u. is associated with symmetry-breaking electron localization [2]. The exact ionization rate, however, has a single broad peak centered between 4 and 5 a.u. and is smaller than that of the clamped-nuclei calculations, but still higher than the atomic rate, similar to the observations in Refs. [4,5].

The nuclear charge distribution (middle panel of Fig. 1) bifurcates; a large fragment of the nuclear density remains localized, oscillating around the equilibrium separation, while another part dissociates, soon after the ionization is onset; c.f. the electronic density plotted in the lower panel. Therefore considering ionization rate simply versus $\langle R \rangle$ does not properly indicate the internuclear separations at which the ionization rate is enhanced. A dynamical picture of CREI accounting for coupling to the nuclear distribution as it changes in time is desirable.

Such a picture is provided within the exact factorization framework [16,17]: in its *reverse* formulation [20], the electron-nuclear wave function $\Psi(\underline{\mathbf{r}}, \underline{\mathbf{R}}, t)$ that solves the full electron-nuclear TDSE can be exactly written as a product $\Psi(\underline{\mathbf{r}}, \underline{\mathbf{R}}, t) = \Phi(\underline{\mathbf{r}}, t)\chi_{\underline{\mathbf{r}}}(\underline{\mathbf{R}}, t)$, where $\Phi(\underline{\mathbf{r}}, t)$ may be interpreted as the electronic wave function and $\chi_{\underline{\mathbf{r}}}(\underline{\mathbf{R}}, t)$ the conditional nuclear wave function that parametrically depends on the electronic configuration $\underline{\mathbf{r}}$ and satisfies the partial normalization condition $\int d\underline{\mathbf{R}} |\chi_{\underline{\mathbf{r}}}(\underline{\mathbf{R}}, t)|^2 = 1$ for every $\underline{\mathbf{r}}$ at each t. The electronic wave function yields the exact N_e-body electronic density and electronic current density of the system. The equations that the electronic and nuclear factors satisfy are presented in [20]. The electronic equation, in particular, has the appealing form of a TDSE that contains an exact TD potential energy surface for electrons (e-TDPES), as well as a TD vector potential: in one dimension, we can choose a gauge such that the vector potential is zero [16,17,20], and then the exact electronic TDSE for our H_2^+ model reads

$$\left(-\frac{1}{2\mu}\frac{\partial^2}{\partial z^2} + \epsilon_e(z,t)\right)\Phi(z,t) = i\partial_t \Phi(z,t), \qquad (2)$$

where

$$\epsilon_e(z,t) = \epsilon^{\mathrm{app}}(z,t) + \mathcal{T}_n(z,t) + \mathcal{K}_e^{\mathrm{cond}}(z,t) + \epsilon_e^{\mathrm{gd}}(z,t) \qquad (3)$$

is the exact potential driving the electron dynamics. The e-TDPES, $\epsilon_e(z,t)$ can be compared with the traditional potentials used to study electronic dynamics and consists of four terms. First, $\epsilon^{\mathrm{app}}(z,t) = \langle \chi_z(R,t)|\hat{W}_{en}(z,R) + \hat{W}_{nn}(R)|\chi_z(R,t)\rangle_R + \hat{V}^l(z,t)$ is an approximate potential generalizing the traditional ϵ^{qs} to the case of a quantum nuclear wave packet [32]. The second term, $\mathcal{T}_n(z,t) = -\langle \chi_z(R,t)|\partial_R^2|\chi_z(R,t)\rangle_R/M$, represents a nuclear-kinetic contribution to the electronic potential from the conditional nuclear wave function, while $\mathcal{K}_e^{\mathrm{cond}}(z,t) = \langle \partial_z \chi_z(R,t)|\partial_z \chi_z(R,t)\rangle_R/\mu$ is an electronic-kinetic-like contribution from the conditional nuclear wave function. Finally $\epsilon_e^{\mathrm{gd}}(z,t) = \langle \chi_z(R,t)|-i\partial_t|\chi_z(R,t)\rangle_R$ is the gauge-dependent component of the potential. Note that ϵ^{app} reduces to ϵ^{qs} when the nuclear density is approximated classically as a z-independent delta function at $\bar{R}(t) = \langle R \rangle(t)$; i.e. $\epsilon^{\mathrm{qs}}(z,t|\bar{R}(t)) = \hat{W}_{en}(z,\bar{R}(t)) + \hat{W}_{nn}(\bar{R}(t)) + \hat{V}^l(z,t)$.

We now investigate the e-TDPES [Eq. (3)] and discuss the impact of its components on the electron dynamics. In particular, we ask how well electron propagation on ϵ^{app} performs: is accounting for the width of the nuclear wave packet, and its correlation with the electron dynamics via the parametric dependence, enough to capture accurately the full electron dynamics? In Fig. 2, the exact e-TDPES, ϵ_e (black solid line) and its four components together with ϵ^{qs} (blue dotted) are plotted on the left-hand side at five different snapshots of time in which the field is at the maximum of the cycle. The exact electron density together with the electron density calculated from propagating the electron on ϵ^{qs} and ϵ^{app} are plotted on the right-hand side. We plot the ionization probabilities [33] calculated from propagating the electron on different components of e-TDPES on the left on Fig. 3.

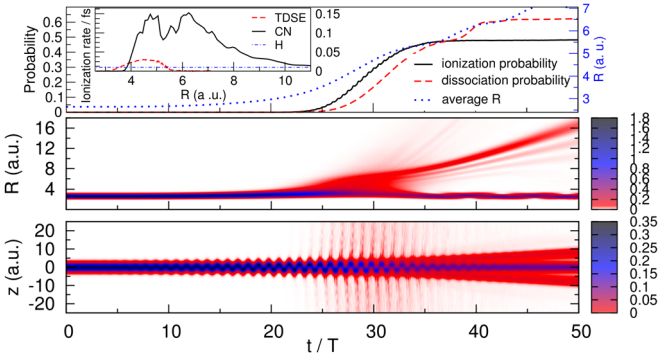

FIG. 1 (color online). Top: average internuclear distance, ionization, and dissociation probability versus number of cycles t/T. The inset depicts the ionization rate for clamped-nuclei (CN) calculation versus R (black dashed line), the full TDSE versus $\langle R \rangle$ (red full line), and the H atom (dash dotted line). Middle (bottom): contour plot of the TD nuclear (electronic) density.

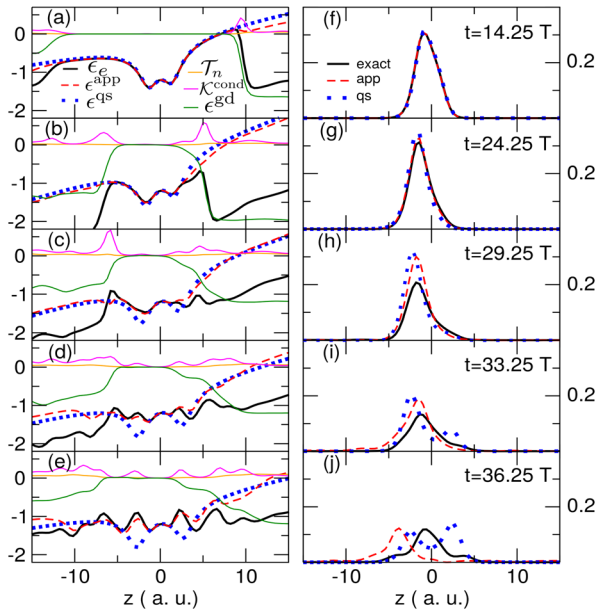

FIG. 2 (color online). Left: exact e-TDPES ϵ_e (black solid line), its various components and $\epsilon^{\rm qs}$ (blue dotted line). For very large z, not shown here, the exact potential is parallel to $\epsilon^{\rm qs}$. Right: exact electron density together with the electron density calculated from propagating the electron on $\epsilon^{\rm qs}$ and $\epsilon^{\rm app}$ at different snapshots of time.

We have chosen times representative of three different phases of the dynamics (refer to Fig. 1): (1) up to $t \approx 20T$, for which the dissociation and ionization probabilities are still negligible [Fig. 2(a)], (2) the second phase, $\sim 20T < t < \sim 35T$, when ionization or dissociation mostly occurs [Figs. 2(b–d)], (3) the final phase, $t > 35T$, in which the system begins to stabilize [panel (e)].

During the first phase, the nuclear wave packet is localized around its initial position and the e-TDPES, $\epsilon^{\rm qs}$, and approximate potentials are essentially on top of each other in the central region ($|z| < 10$ a.u.), differing only in the tail, where, in particular, ϵ_e has a large step downward [Fig. 2(a)]. The position of the drop corresponds

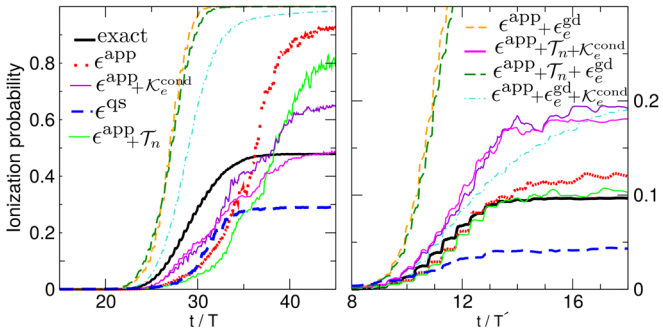

FIG. 3 (color online). Ionization probabilities calculated from propagating the electron on different components of the exact electronic potential as well as on the quasistatic potential. Left: $\lambda = 800$ nm and $I = 2 \times 10^{14}$ W/cm^2 (50-cycle). Right: $\lambda = 600$ nm and $I = 10^{14}$ W/cm^2 (20-cycle). Legends apply to both.

to a sharp change in the z dependence of the conditional nuclear wave function. Since the density is tiny in the tail region, the overall dynamics is not affected significantly by this feature. In the second phase of the dynamics the nuclear motion begins to pick up, affecting the shape of the exact e-TDPES in the central region. From this point on the exact potential develops features that are absent in $\epsilon^{\rm qs}$ and $\epsilon^{\rm app}$. As part of the nuclear density begins to stretch apart, the e-TDPES exhibits a double well structure in the up-field side of the potential ($0 < z < 5$ a.u.), while the down-field side maintains a single well, as is evident in panels (b) and (c). Further, the depth of the central wells are decreased compared to $\epsilon^{\rm qs}$. Outside the central region ($|z| > 5$ a.u.) the e-TDPES drops down, yielding a barrier that is smaller and narrower than that of $\epsilon^{\rm qs}$. This feature, in particular, significantly facilitates the tunnelling ionization of the electron density in the exact dynamics already at $t = 24.25T$, evident in the spreading of the exact density [panel (g); see also left panel of Fig. 3]. In the case of the quasistatic and approximate potentials, the ionization is still negligible at this time, due to a small tunnelling probability. The differences between the exact e-TDPES and both $\epsilon^{\rm app}$ and $\epsilon^{\rm qs}$ continue to grow in the central region ($|z| < 5$ a.u.) throughout the second phase [panels (b–d)], and corresponding electronic densities [(g–i)] as contributions from $\epsilon_e^{\rm gd}$ and $\mathcal{K}_e^{\rm cond}$ increase and extend closer to the center. It is interesting that $\epsilon_e^{\rm gd}$ typically has large steps that lowers the potential on both sides, allowing for more ionization (see also Fig. 3, left panel), while $\mathcal{K}_e^{\rm cond}$ develops several (smaller) barrier structures, whose net effect also appears to increase the ionization probability in this phase (see Fig. 3). The $\mathcal{T}_n$ term has very small barriers in the outer region whose tendency is to confine the density, leading to a decrease in the ionization probability.

By the end of the second phase, at $t = 33.25T$ [Fig. 2(d)], the exact potential is totally different from $\epsilon^{\rm qs}$, everywhere except for $|z| < 1$, presenting a shallow double well structure in both up-field and down-field sides of the potential. Furthermore, the discrepancy between the $\epsilon^{\rm qs}$ and $\epsilon^{\rm app}$ becomes more noticeable as the nuclear wave packet splits and dissociates in the field. By this time, there has been significant ionization in all three cases (left panel of Fig. 3), although more in the exact case. Towards the end of the second phase, the ionization probabilities of the quasistatic and approximate calculations differ from each other, as expected from the growing discrepancy between their respective potentials.

Entering the third phase of the dynamics [Fig. 2(e)], the exact potential differs dramatically from the other two forming four wells in the central region ($|z| < 6$ a.u.). The two wells in the center are associated with the nuclear density localized around the equilibrium while the other two are associated with the dissociating fragment and move outwards. The e-TDPES consequently localizes the electronic density in three positions as seen in Fig. 2(j), namely,

in the center and on each of the dissociating fragments of protons. In the third phase, $\epsilon^{\rm app}$ grossly overionizes the system—as $\epsilon^{\rm app}$ has many shallow barriers and continues to oscillate in the field, failing to stabilize. The $\epsilon^{\rm qs}$ retains a deep double well structure throughout the dynamics, in contrast to the exact; toward the end of the pulse the ionization in either of these cases saturates, but the quasistatic fails to get the density and ionization probability correct.

The left panel of Fig. 3 shows that neglecting all the electron-nuclear correlation terms except for $\epsilon^{\rm app}$ underestimates the ionization at first, but later, as the exact ionization begins to saturate, the ionization from $\epsilon^{\rm app}$ continues to grow, and leads ultimately to a significant overestimate of the total ionization. Even propagating on $\epsilon^{\rm qs}$, a crude approximation given in the earlier discussion, gives a better ionization probability.

We see from Fig. 3 (left) that adding $\mathcal{T}_n$ to $\epsilon^{\rm app}$ reduces the ionization probability at all times, due to its small confining barriers as mentioned above. On the other hand, adding $\mathcal{K}^{\rm cond}$ to $\epsilon^{\rm app}$ increases the ionization at first, and then decreases it, giving an overall somewhat improved prediction of the ionization dynamics relative to dynamics on $\epsilon^{\rm app}$ alone. Although adding both $\mathcal{K}^{\rm cond}$ and $\mathcal{T}_n$ to $\epsilon^{\rm app}$ seems to give a good final ionization probability, the intermediate dynamics is not good. Adding $\epsilon_e^{\rm gd}$ to $\epsilon^{\rm app}$ drastically overshoots the ionization, yielding ultimately a complete ionization. For the current choice of laser parameters and initial state all these dynamical electron-nuclear correlation terms are important to include to obtain good prediction of the ionization probability. But is this conclusion general? Does $\epsilon^{\rm app}$ always perform so poorly?

We performed the same calculations using a 20-cycle pulse of wavelength $\lambda = 600$ nm and intensity $I = 10^{14}$ W/cm^2, with a sine-squared pulse envelope, setting the initial state to be the sixth excited vibrational state (cf. [4]). The ionization probabilities computed from propagating the electron on different components of the exact potential is presented in the right panel of Fig. 3 ($T' = 2$ fs is the duration of one cycle). Electron dynamics on $\epsilon^{\rm app}$ in this case agrees very well with the exact result that with the addition of $\mathcal{T}_n$ [34] to $\epsilon^{\rm app}$ becomes even better. Other combinations of the potential components do not provide satisfactory results. The quasistatic dynamics underestimates the ionization probability significantly: the exact potential differs substantially from $\epsilon^{\rm qs}$ from the start due to the vibrational excitation of the initial state.

It is clear that ionization dynamics depends crucially on coupling to quantum nuclear motion; accounting for both the splitting of the wave packet as well as its dynamics is important. From which part of the nuclear wave packet is the ionization mostly occurring? To answer this, we plot a time-resolved, R-resolved ionization probability [35] via $I(R,t) = \int_{z_I'} dz |\Psi(z,R,t)|^2$, with $\int_{z_I'} = \int_{-\infty}^{-z_I} + \int_{z_I}^{\infty}$ and $z_I = 15$ a.u., in Fig 4 for *both* of the laser

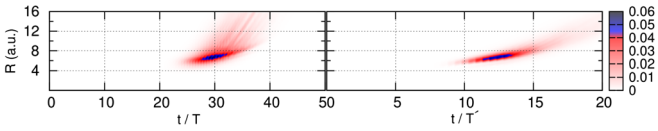

FIG. 4 (color online). Time-resolved, R-resolved ionization probability, $I(R,t)$. Left: $\lambda = 800$ nm and $I = 2 \times 10^{14}$ W/cm^2 (50-cycle). Right: $\lambda = 600$ nm and $I = 10^{14}$ W/cm^2 (20 cycle).

parameters studied in this work. In both cases, we observe a clear peak of $I(R,t)$, centered around 6 a.u. $< R <$ 7.5 a.u., the region predicted by the quasistatic analysis of CREI, soon after the fields reach their maximum intensities. Hence, the quantity $I(R,t)$ represents a very useful measure of CREI in a fully dynamical picture, indicating clearly the dominant internuclear separations at which ionization occurs. This quantity is analogous to the ionization probability at a given internuclear separation in the quasistatic picture (see Supplemental Material [36]).

In summary, we have found the exact potential driving the electron dynamics in a model one-dimensional H_2^+ molecule undergoing CREI. The potential provides complete details of the CREI process beyond the quasistatic picture traditionally used to analyze and interpret CREI. The large differences in the two potentials, and the resulting dynamics, reveals the importance of dynamical electron-nuclear correlation terms lacking in previous pictures of CREI: propagating the electrons in a potential that neglects these terms gives large errors in the predictions of the ionization probability. Going beyond the quasistatic treatment by only accounting for the width and splitting of the nuclear wave packet is generally not enough to get the correct dynamics of CREI. How significant the dynamical electron-nuclear effects are for CREI phenomena in larger systems [37] remains to be investigated. In many-electron systems, the potential is a function of all electronic coordinates. How to accurately model this potential opens a major avenue for future research. One direction is to develop a time-dependent density-functional approach for the coupled systems, that deals with a one-electron Kohn-Sham equation coupled to nuclear degrees of freedom [38]. Another direction would be based on writing an N-particle wave function as a product of N one-particle functions as proposed in [39]. Future efforts to treat the nuclear dynamics efficiently will explore approximations for the conditional nuclear wave function, e.g. stemming from a time-dependent Born-Oppenheimer similar to Ref. [40] but in an reverse formulation. Finally we showed a time-resolved, R-resolved measure of CREI that accounts for the dynamical electron-nuclear correlation has a clear peak in the region predicted by the quasistatic analysis.

Financial support from the National Science Foundation CHE-1152784 (N. T. M), and Department of Energy, Office of Basic Energy Sciences, Division of Chemical

Sciences, Geosciences and Biosciences under Award DE-SC0008623, the European Research Council Advanced Grant DYNamo (ERC- 2010-AdG-267374) and Grupo Consolidado UPV/EHU del Gobierno Vasco (IT578-13) (E. K, A. A.) are gratefully acknowledged.

*Corresponding author.
elham.etn@gmail.com
†aliabedik@gmail.com
‡nmaitra@hunter.cuny.edu

[1] T. Zuo, S. Chelkowski, and A. D. Bandrauk, Phys. Rev. A **48**, 3837 (1993).
[2] T. Zuo and A. D. Bandrauk, Phys. Rev. A **52**, R2511 (1995).
[3] T. Seideman, M. Y. Ivanov, and P. B. Corkum, Phys. Rev. Lett. **75**, 2819 (1995).
[4] S. Chelkowski, A. Conjusteau, T. Zuo, and A. D. Bandrauk, Phys. Rev. A **54**, 3235 (1996).
[5] I. Ben-Itzhak, P. Q. Wang, A. M. Sayler, K. D. Carnes, M. Leonard, B. D. Esry, A. S. Alnaser, B. Ulrich, X. M. Tong, I. V. Litvinyuk, C. M. Maharjan, P. Ranitovic, T. Osipov, S. Ghimire, Z. Chang, and C. L. Cocke, Phys. Rev. A **78**, 063419 (2008).
[6] E. Constant, H. Stapelfeldt, and P. B. Corkum, Phys. Rev. Lett. **76**, 4140 (1996).
[7] J. Wu, M. Meckel, L. P. H. Schmidt, M. Kunitski, S. Voss, H. Sann, H. Kim, T. Jahnke, A. Czasch, and R. Dörner, Nat. Commun. **3**, 1113 (2012).
[8] S. Chelkowski, C. Foisy, and A. D. Bandrauk, Phys. Rev. A **57**, 1176 (1998).
[9] S. Chelkowski and A. Bandrauk, J. Phys. B **28**, L723 (1995).
[10] H. Yu, T. Zuo, and A. D. Bandrauk, J. Phys. B **31**, 1533 (1998).
[11] A. D. Bandrauk and F. Légaré, in *Progress in Ultrafast Intense Laser Science VIII* (Springer, New York, 2012), pp. 29–46.
[12] S. Hammes-Schiffer and A. V. Soudackov, J. Phys. Chem. B **112**, 14108 (2008).
[13] N. Takemoto and A. Becker, Phys. Rev. Lett. **105**, 203004 (2010).
[14] N. Takemoto and A. Becker, Phys. Rev. A **84**, 023401 (2011).
[15] F. Légaré, I. V. Litvinyuk, P. W. Dooley, F. Quéré, A. D. Bandrauk, D. M. Villeneuve, and P. B. Corkum, Phys. Rev. Lett. **91**, 093002 (2003).
[16] A. Abedi, N. T. Maitra, and E. K. U. Gross, Phys. Rev. Lett. **105**, 123002 (2010).
[17] A. Abedi, N. T. Maitra, and E. K. U. Gross, J. Chem. Phys. **137**, 22A530 (2012).
[18] A. Abedi, N. T. Maitra, and E. K. U. Gross, J. Chem. Phys. **139**, 087102 (2013).
[19] A. Abedi, F. Agostini, Y. Suzuki, and E. K. U. Gross, Phys. Rev. Lett. **110**, 263001 (2013).
[20] Y. Suzuki, A. Abedi, N. T. Maitra, K. Yamashita, and E. K. U. Gross, Phys. Rev. A **89**, 040501 (2014).
[21] A. Abedi, F. Agostini, and E. K. U. Gross, Europhys. Lett. **106**, 33001 (2014).
[22] S. K. Min, A. Abedi, K. S. Kim, and E. K. U. Gross, Phys. Rev. Lett. **113**, 263004 (2014).
[23] Y. Suzuki, A. Abedi, N. Maitra, and E. K. U. Gross, Phys. Chem. Chem. Phys. **17**, 29271 (2015).
[24] F. Agostini, A. Abedi, Y. Suzuki, S. K. Min, N. T. Maitra, and E. K. U. Gross, J. Chem. Phys. **142**, 084303 (2015).
[25] S. K. Min, F. Agostini, and E. K. U. Gross, Phys. Rev. Lett. **115**, 073001 (2015).
[26] G. Hunter, Int. J. Quantum Chem. **9**, 237 (1975).
[27] N. I. Gidopoulos and E. K. U. Gross, Phil. Trans. R. Soc. A **372**, 20130059 (2014).
[28] L. S. Cederbaum, J. Chem. Phys. **138**, 224110 (2013).
[29] R. Lefebvre, J. Chem. Phys. **142**, 074106 (2015).
[30] J. Javanainen, J. H. Eberly, and Q. Su, Phys. Rev. A **38**, 3430 (1988).
[31] G. J. Halász, Á. Vibók, and L. S. Cederbaum, J. Phys. Chem. Lett. **6**, 348 (2015).
[32] Here $\hat{W}_{en}$ is a summation of the third and fourth term of Eq. (1), while $\hat{W}_{nn}$ is its fifth term.
[33] Steps in the ionization probability for both cases are associated with the multiple ionization bursts within each optical cycle [13].
[34] Note that $\mathcal{T}_n$ is inversely proportional to the nuclear mass; therefore, it is likely less pronounced for heavier nuclei.
[35] K. C. Kulander, F. H. Mies, and K. J. Schafer, Phys. Rev. A **53**, 2562 (1996).
[36] See Supplemental Material at http://link.aps.org/supplemental/10.1103/PhysRevLett.115.263002 for details of the calculations.
[37] I. Bocharova, R. Karimi, E. F. Penka, J.-P. Brichta, P. Lassonde, X. Fu, J.-C. Kieffer, A. D. Bandrauk, I. Litvinyuk, J. Sanderson *et al.*, Phys. Rev. Lett. **107**, 063201 (2011).
[38] T. Kreibich and E. K. U. Gross, Phys. Rev. Lett. **86**, 2984 (2001).
[39] L. S. Cederbaum, Chem. Phys. **457**, 129 (2015).
[40] L. S. Cederbaum, J. Chem. Phys. **128**, 124101 (2008).